RSC Advances

PAPER

View Article Online
View Journal | View Issue

Cite this: RSC Adv., 2015, 5, 56677

Nanospot welding of carbon nanotubes using near-field enhancement effect of AFM probe irradiated by optical fiber probe laser†

Lijun Yang,‡[a] Jianlei Cui,‡*[abc] Yang Wang,*[a] Chaojian Hou,[a] Hui Xie,[d] Xuesong Mei,[b] Wenjun Wang[b] and Kedian Wang[b]

Received 10th September 2014
Accepted 23rd June 2015

DOI: 10.1039/c4ra10117k

www.rsc.org/advances

The miniaturization of electronic devices into the nanometer scale is indispensable for next-generation semiconductor technology, and carbon nanotubes are considered to be the promising candidates for the future interconnection wires. To study carbon nanotube interconnection during nanowelding, we propose a new nanospot welding method with the near-field enhancement effect of the metallic AFM probe tip irradiated by an optical fiber probe laser. Based on theoretically analyzing the near-field enhancement effect, we set up the experimental system for nanospot welding with good interconnection results of silver nanoparticles and carbon nanotubes, not only proving that the interconnection operation of CNTs can be effectively achieved through the melting process of nanoparticles by the thermal AFM probe tip irradiated by an optical fiber probe laser, but also providing a promising technical approach for nanospot welding.

1. Introduction

According to the latest International Technology Roadmap for Semiconductors (ITRS),[1] the miniaturization of electronic devices into the nanometer scale is indispensable for next-generation semiconductor technology. Due to obvious electro-migration with smaller feature size, carbon nanotubes (CNTs)[2] are considered to be the promising candidates for future interconnect wires of next-generation electronic devices with excellent physical and chemical properties ranging from ultra-high mechanical strength, to electrical and thermal properties, *etc.*[3–9] And properly joined CNTs could be the building blocks of various electronic devices. Therefore, there has been much research aimed at exploring the production of a junction formed by CNTs.[10–14]

For the excellent junction, some effective methods have been adopted for CNTs welding.[15–31] For example, Terrones *et al.*[15] and Krasheninnikov *et al.*[18,19] studied the formation of the CNTs junction with electron beam and ion beam, respectively. But, the when CNTs are irradiated by high energy beam, the atomic structures of CNTs have large damages to induce high contact resistance and weak mechanical strength, which limits the practical applications. As chemical vapor deposition (CVD) method,[20] the sophisticated templates are needed in welding process. And CVD method does not solve the interconnection between CNT and CNT, and become the main tool for the interconnection between carbon nanotube bundles and electrode, which is similar to the ultrasonic welding method.[21] To overcome the adverse effects, nano-welding method with thermal treatment, has been founded as a more effective method with favorable electrical and thermal properties of the junction. Dockendorf *et al.*[23,24] deposited a gold nanoparticle suspension (nanoink) film on the area where the carbon nanotube contacts the metal pad based on the fountain-pen principle. The interconnection between CNTs and electrode was accomplished after annealing and sintering of the nanoink placed on the hot plate. Wu *et al.*[25] performed carbon nanotube bundles welding experiments under vacuum condition with temperature range from 780 to about 815 °C. But, the all nanowires or micro/nano structures on the chip are easy to be damaged by overall heating of substrate. So nanospot welding method is becoming the major solution. And by nanoscale electrical welding method with Joule heat, Peng *et al.*[26] reported that individual metallic nanowires and nanoobjects can be assembled and welded together using sacrificial metal nanowire solder based on manipulation and interconnection process under two nanoprobes system. However, solder deposition on intercontacted nanowires process requires complex and precise

[a]Key Laboratory of Micro-systems and Micro-structures Manufacturing, Ministry of Education, Harbin Institute of Technology, Harbin 150001, P. R. China. E-mail: cjlxjtu@mail.xjtu.edu.cn

[b]State Key Laboratory for Manufacturing Systems Engineering, Xi'an Jiaotong University, Xi'an 710049, P. R. China

[c]State Key Laboratory of Surface Physics and Department of Physics, Fudan University, Shanghai 200433, P. R. China

[d]State Key Laboratory of Robotics and Systems, Harbin Institute of Technology, Harbin 150001, P. R. China

† Electronic supplementary information (ESI) available. See DOI: 10.1039/c4ra10117k

‡ Authors contributed equally to this work.

nanomanipulation system, and sacrificial metal nanowire solder will inevitably cause some impacts on nanostructures near the junction in the future application.

Since the scanning tunneling microscopy (STM) was developed, it led to the invention of a series of scanning probe techniques, such as atomic force microscopy (AFM), scanning near-field optical microscopy (SNOM), and further variants thereof, which have not only become indispensable tools for surface imaging but have also offered a promising method for the modification of surface.[32–34] Based on the laser-assisted patterning with AFM and the situation of CNTs nanowelding technology described herein, for the first time, here we propose a new nanospot welding method for CNTs nanospot interconnection based on the near-field enhancement effect of AFM probe irradiated by optical fiber probe laser, and demonstrate the effectiveness and feasibility of nanospot welding in this paper.

2. Theoretical analysis and discussion

In this new nanospot welding method, the key advance is to achieve the melting process of nano-welding material using the AFM probe heated by laser. As the scheme of the spatial focused laser irradiating AFM probe, due to the diffraction limit and alignment operation problem between laser and AFM probe, nanostructures and nanodevices are easily modified and damaged by spatial focused laser with larger spot size of several microns based on near-field enhancement effect of nanomaterials and nanostructures. In addition, laser accurately irradiating AFM probe tip, not affecting the whole probe or its cantilever, is difficult to be achieved from design to build of experimental system without flexibility. Consequently, based on the laser thermal theory and near-field enhancement effect, the heating process is achieved through optical fiber probe laser irradiating the AFM probe tip. And the principle of the process is illustrated in Fig. 1a. The laser can be transmitted by the fiber and be focused by optical fiber probe. And the light reflected from the tapered metalized probe tip is propagated to the optical fiber and directed by the fiber splitter to a power meter for detection. The back-reflected light at the detector consists of a small depolarized component due to the polarization scrambling nature of the fiber. This light is optimized to ensure that the laser beam is efficiently coupled into the core with the diameter of several micrometers and then directed all the way to the fiber tip. The combination of flange attenuator and the polarization rotator permits that continuous variation of the laser power and polarization is suited for the controllable nanospot welding process. The optical fiber probe, placed in guide unit to avoid vibration, is attached to a multi-dimensional nanopositioning stage, and then inserted into the substrate on the sample object stage. As the optical system, all-fiber coupling optical circuit with low loss can match the optical fiber probe well due to the good transmission. Therefore, the spatial light path is very flexible, and in the procedure of nanospot welding, the relative position between the AFM probe tip and optical fiber probe can be ensured by multi-dimensional positioning stage with high accuracy. Simultaneously, the AFM probe tip can be irradiated by optical fiber probe laser for the following nanospot welding of CNTs, and the corresponding experimental system for nanointerconnection is shown in Fig. 1b. In the nano-welding process, forming the junction between the carbon nanotubes with nano-welding material, need to ensure that the temperature of nano-welding material reaches its melting point. However, laser is an electromagnetic wave of shorter wavelength with high intensity, if the AFM probe is irradiated by laser, the electric field will heat the AFM probe. And the heat source item can be obtained by classical electromagnetic theory, which is as follow.

$$Q = \frac{\omega_l}{8\pi}\varepsilon''_t|\boldsymbol{E}|^2 \quad (1)$$

where, ω_l gives the frequency of incident laser, ε''_t is the imaginary part of relative permittivity of AFM probe, $\boldsymbol{E}$ shows the electric field strength.

Visibly, the thermal field solution can be translated into the electric field problem, so first of all, the electric and thermal field of AFM probe was subsequently studied from the theoretical analysis for the temperature of AFM probe during the nano-welding, respectively.

According to the near-field optical theory,[35–38] if the incident laser emits through the optical fiber probe, the enhanced electric field appears at the confined aperture region. Further, if the AFM metallic probe tip is irradiated by the near-field light, the secondary enhancement phenomenon produced around the AFM probe tip, and the enhanced electric field can affect the thermal field distribution. To study the enhanced electric field, Fig. 2a shows the computational model of AFM metallic probe irradiated by a tapered metal-coated optical fiber probe laser. In the model, the incident laser transmits along the x-axis direction with the polarization direction along the z-axis direction. The core of optical fiber probe with SiO_2 material is coated by Al film. According to the actual parameters of optical fiber probe, the larger end diameter of probe φ_1, smaller end diameter φ_2, and the length H was set to ~700 nm, 100 nm, and 600 nm, respectively. And the curvature radius R_t, taper angle θ_t of AFM probe tip of Si material coated with Pt film, was set to 20 nm, 30°, respectively. In order to obtain the near-field enhancement effect of AFM probe tip, the AFM probe was placed in the near-field region of optical fiber probe, and the distance was set to 60 nm between the centerline position of AFM probe and aperture end of optical fiber probe. In the computation of the near-field enhancement, the wavelength of the incident laser plays an important role, which was analyzed in our previous report.[39] So laser wavelength was set to 808 nm based on the wavelength of actual incident laser. In addition, to calculate the enhancement characteristics at the corresponding laser wavelength. The refractive index of optical fiber laser core n_{SiO2}, the permittivity of ε_{Al}, ε_{Si} and ε_{Pt} was set to 1.5, −34.5 + i8.5, 13.6 + i0.044, and −17.179 + i29.609, respectively.[40] Because the penetration depth of light on aluminum material is very small, the thickness of aluminum film T was set to 80 nm in order to ensure the limitation of scattering and transmitting light, combining the actual metal layer parameters of optical fiber probe.

In this near-field simulations of AFM probe irradiated by optical fiber probe laser, the field enhancement factor (FEF),[41]

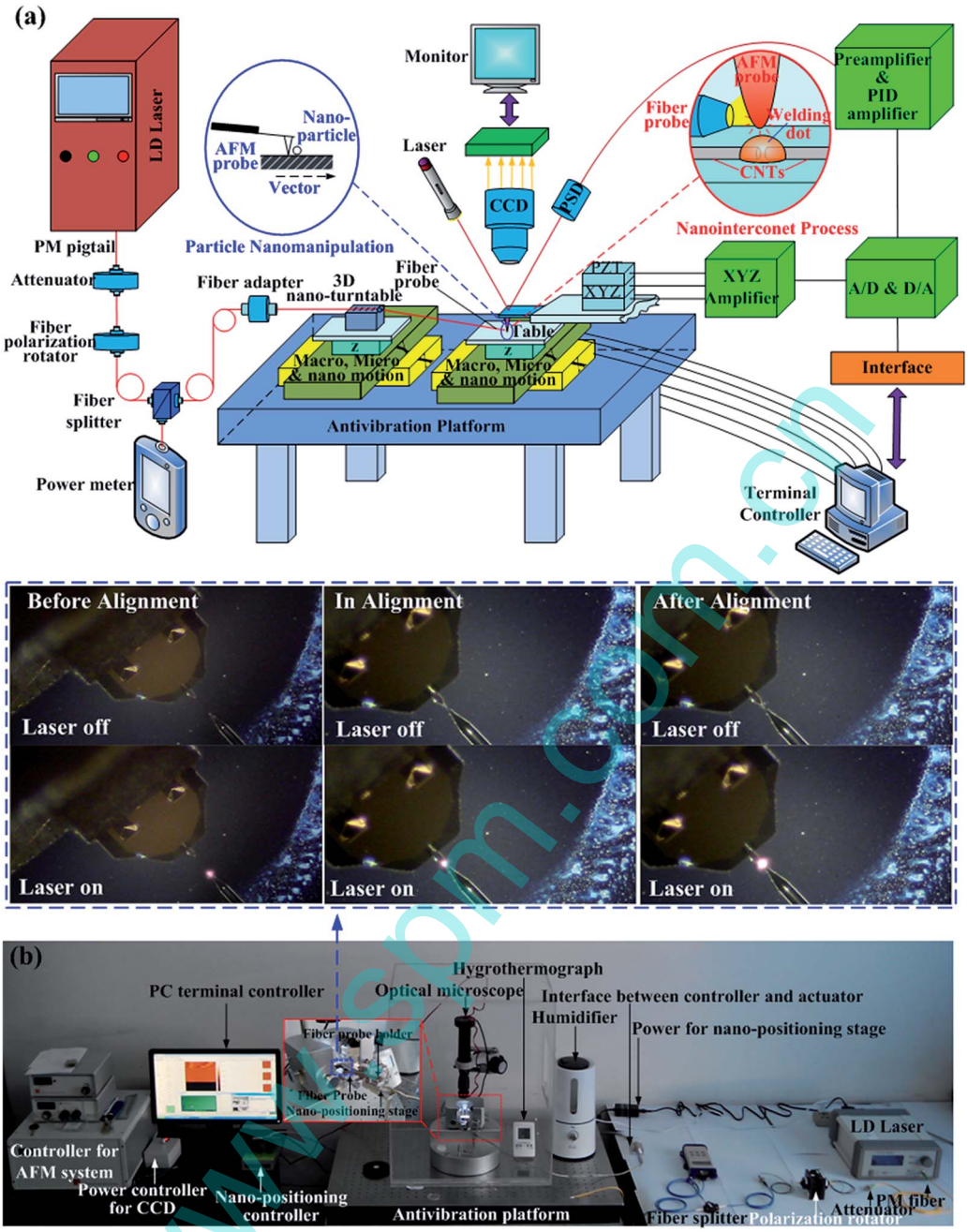

Fig. 1 (a) Schematic diagram and (b) experimental system for nanointerconnection with AFM system and the focused optical fiber probe laser.

defined as the ration E_t/E_0 (E_t gives the enhanced electric field amplitude at the AFM probe tip, and E_0 denotes the electric field amplitude of the incident laser), was chosen to measure the near-field enhancement effect. For clearly and simply expressing the FEF, the electric field amplitude of the incident laser E_0 was set to 1 V m^{-1}, so the electric field amplitude E_t is equal to the FEF value at the corresponding position.

Based on the computational model, to analyze the near-field effect of metallic AFM probe irradiated by laser, it was simulated with finite element method and Fig. 2b shows the electric field distribution. According to the waveguide theory, when laser enters into the optical fiber probe, the transmission problem will be transformed into a metal waveguide propagation problem. The outer metal cladding layer can prevent laser leakage with high reflectivity and good binding ability to the laser. During the laser transmitting into the optical fiber probe tip, part of the laser is reflected by the inner side of the cladding layer and superimposed with the incident laser to form a strong standing wave field along the x-axis direction. With the transmission into the aperture of fiber probe, the diameter of probe is gradually reduced, so the light with various modes is individually turned off, remaining the HE_{11} mode laser in the transmission process. And when the diameter of probe is reduced to the cut-off diameter of HE_{11} mode light, the HE_{11}

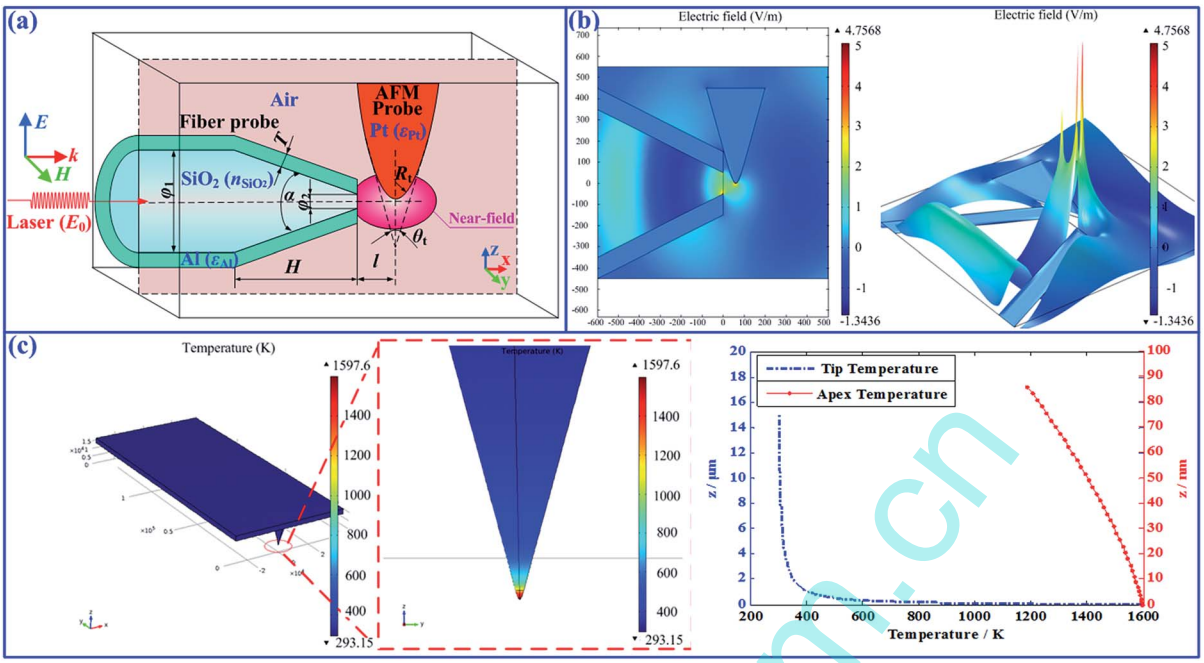

Fig. 2 (a) Computational model of the metallic AFM probe irradiated by a tapered metal-coated optical fiber probe with the simulation results of (b) electric field and (c) thermal field of AFM probe.

mode laser will also be cut-off with light vector becoming the imaginary. At the same time, the electric intensity has the extreme value at the −200 nm position along the *x*-axis direction, which is consistent with the theoretical formula about the cut-off wavelength λ_c of HE_{11} mode laser as follow:

$$\lambda_c = 2\pi a/1.84 \quad (2)$$

here, *a* gives the radius of circular waveguide.

Because the wavelength of incident laser is 808/1.5 nm in SiO_2 medium, the cut-off diameter is about 315 nm, which is approximately equal to diameter of optical fiber probe at the −200 nm position along the *x* direction with proving the correctness of the simulations. Then, the laser, passing through the cut-off plane, continues to decay. However, at the outlet portion of optical fiber probe, the field strength increases due to the near-field enhancement effect based on surface plasmon resonance, with reaching the maximum values at the sharp boundary portion of optical fiber probe and AFM probe tip. And the surface plasmon resonance and edge enhancement phenomenon affect the electric field distribution of the metallic AFM probe with the secondary enhancement phenomenon of the FEF value as high as 4.7568. According to the near-field distribution in Fig. 2b, due to the mutual influence of the surface plasmon and the positional relation between the optical fiber probe and the AFM probe, the near-field distribution is asymmetry on the centerline of optical fiber probe and AFM probe.

Since the AFM probe tip is irradiated by the laser, the thermal field can be formed, and the enhanced electric distribution can subsequently affect the thermal field distribution.[42,43] As an electromagnetic wave, laser has high energy which is determined by Poynting vector as follow:

$$\boldsymbol{S} = \boldsymbol{E} \times \boldsymbol{H} \quad (3)$$

here, $\boldsymbol{S}$ denotes the Poynting vector, $\boldsymbol{E}$ and $\boldsymbol{H}$ is the electric intensity and magnetic intensity, respectively.

In addition, the $\boldsymbol{H}$ can be replaced by $\boldsymbol{E}$ based on the Maxwell equations. Therefore, the electromagnetic energy size of Poynting vector can be expressed by the following formula.

$$I = \boldsymbol{S} = 0.5c\varepsilon_0 nE^2 \quad (4)$$

here, *I* is the light intensity, *c* gives the velocity of light, ε_0 and *n* indicates the dielectric constant of vacuum and the refractive index of the medium respectively.

So the heat source per unit volume can be expressed by the following equation.

$$\dot{q} = I\alpha \quad (5)$$

where

$$\alpha = 4\pi k/\lambda \quad (6)$$

here, α, *k*, and λ is the absorption rate, extinction coefficient, and wavelength, respectively.

Now, combining the electric intensity of AFM probe and heat source equation, the heat source item of heating the AFM probe can be solved, then the thermal field of AFM probe was simulated for getting the distribution characteristics. At the same time, considering the actual parameters of optical fiber probe, AFM probe and laser, the effective laser intensity can be calculated with the value higher than the 1.5×10^{11} W m^{-2} with the enhanced electric field strength. In the simulation process, if

the heat flux, applied to the AFM probe tip according to the Rayleigh length, was set to 1.5×10^{11} W m^{-2}, the AFM probe tip can achieve the stable temperature of 1597.5 K which is higher the melting point of silver nano-welding material in experiments. In addition, Fig. 2c shows that the heat is mainly focused on the tip due to the near-field distribution. Then, if the thermal AFM probe is used to nano-welding process, the nano-welding material can melt to link the adjacent CNTs. Therefore, based on the experimental system in Fig. 1b, the nanospot welding experiments of nano-welding particles were performed to testify the temperature of the thermal AFM probe for the subsequent nanointerconnection of CNTs.

3. Experiments and discussion

Before the welding experiments of nanoparticles, for the adjustable laser power, the single-mode polarized laser instrument (Lumics LU0808M100, Connect laser, China) was selected for incident laser source with the maximum power of 64 mW. The optical fiber probe (MF004, NT-MDT, Russia) was made of a single mode tapered probe with an aperture diameter of 100 nm. In order to adjust the position between optical fiber probe and AFM probe, the optical fiber probe was adhered to a metallic syringe needle which was attached to a three-dimensional nanopositioning stage with ultrahigh resolution of 1 nm (SLC-1720-s, SmarAct, Germany). In addition, the position of sample was scanned *in situ* by scanning probe microscope (SPM) platform (CSPM 5500, Beijing Being Nano-Intruments Ltd., China) with structural transformation of hardware and secondary development of software. In the preparation of nanospot welding, the Si material was selected as substrate surface which needs cleaning process in order to avoid the impact of the dirt, oil, *etc.* In the cleaning process, Si substrate, sequentially put into the centrifuge tube filled with acetone, ethanol absolute and deionized water, was treated with ultrasonic method about 20 minutes, respectively. Then, in order to increase the hydrophilic property of silicon surface, the silicon substrate was boiled through the magnetic stirrer instrument at the temperature of 100 °C, in the mixed solution of H_2O_2 and $NH_3 \cdot H_2O$ according to the volume ratio of 5 : 1. Hereafter, the silicon substrate was washed with the deionized water through ultrasonic instrument and dried with the flow of N_2, becoming the substrate surface for nano-welding process. What's more, considering the excellent electrical property of silver material, silver nanoparticles of 15–20 nm (DK101-1, Beijing DK nano technology Co. LTD, China) were selected as the nano-welding material. And in the preparation for samples, the silver nanoparticles power was diluted with ethanol absolute according to the mass ratio of 1 : 1000. To prevent the agglomeration of silver nanoparticles, the mixed solution was treated for dispersion with ultrasonic instrument about 2 hours, accompanying the heating operation at approximate 50 °C for better dispersion effect. Then, after 10 minutes' standing, supernatant liquid, in the centrifuge tube, was injected with discharge gun, coated on the clean silicon surface with spin coater, and dried with flow of N_2. And the nanoparticles, shown in Fig. 3a, can be got for nanospot welding process under the scanning imaging process of AFM system with tapping mode.

In the nano-welding experiments of nanoparticles, the alignment operation was performed between optical fiber probe and AFM probe tip through the motion of 3-D nanopositioning stage and the angle of optical fiber probe holder, which is shown in Fig. 1b. First, before alignment, the optical fiber probe was manipulated to near the visual AFM probe. When the distance is small between optical fiber probe and AFM probe, the two probes can be observed through optical microscope. And the optical fiber probe was manipulated in the horizontal direction to make the two probes approximation. Then, as the key step of alignment operations, the AFM system was open for scanning and imaging, and the optical fiber probe was manipulated at the same time in the vertical direction. When slippage phenomenon of the fiber probe occurred on the substrate surface along the horizontal direction, it shows that the optical fiber probe was contact with the substrate surface. Because the working principle for scanning and imaging is based on the ultra-fine motion of piezoelectric ceramics with static AFM probe, the optical fiber probe and substrate moved together. In addition, the optical fiber probe was slowly lifted step by step with the ultra-fine motion of three-dimensional nanopositioning stage. When the motion relationship, between optical fiber probe and substrate, was changed from relatively static state to relative motion state, stop lifting probe and maintain the height, and shut down the AFM system and reduce the motion platform at the same time. Now the optical fiber probe tip and the AFM probe tip are in the same height. Finally, for maintaining the small gap between optical fiber probe and AFM probe tip, the optical fiber probe needed to be further manipulated towards the AFM probe tip step by step with the resolution of 1 nm based on the three-dimensional nanopositioning stage. If the AFM probe was suffered from pushing force of optical fiber probe, the contact information between AFM probe and optical fiber probe, can be learned from the second developed monitoring software window. When the changes of the force curve occurred in the monitoring window, it shows that optical fiber probe was in contact with the AFM probe. At the this time, for the specified distance between optical fiber probe tip and AFM probe tip, the optical fiber probe needed to be moved backward according to the specified distance. So the distance between two probes can be effectively controlled, and the AFM probe tip can be illuminated by the optical fiber probe laser after effective alignment.

For getting the nano-welding effect, the agminate silver nanoparticles were chosen as operation objects, and their center, marked with the red crossing lines in Fig. 3a, became the location of AFM probe tip before laser irradiating the AFM probe tip. Accompanying acquisition and conversion of coordinate values in original AFM image, the AFM probe tip can be operated at the predetermined position through relatively moving the piezoelectric ceramics stage with samples. Because the size effect on melting of silver nanoparticles was studied with molecular dynamics method in our previous report,[44] the nanoparticles of 15 nm have high melting temperature of approximately 1100 K. In the nano-welding process, the laser

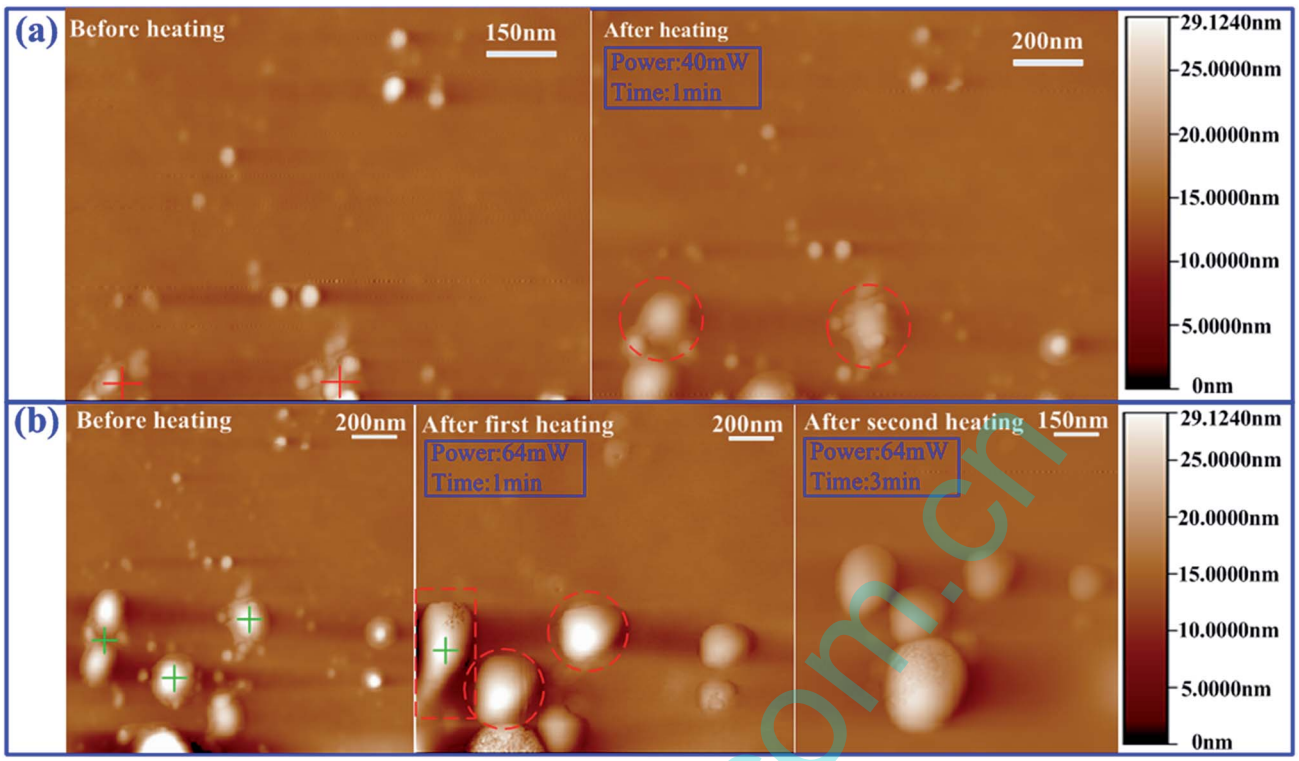

Fig. 3 Experiments for interconnection of silver nanosolders based on AFM probe tip illuminated by fiber probe laser with (a) smaller power of 40 mW and (b) higher power of 64 mW.

power and duration time was controlled at 40 mW and 1 minute respectively, and the nano-welding result is shown in Fig. 3a. The nanoparticles, near the thermal point of AFM probe tip, were sintered into a mound. In contrast, the nanoparticles, away from the hot spot, still kept the monomer morphology. Further, based on the above nanospot welding result, the laser power was increased to 64 mW and applied to the subsequent experiments. And the nanoparticles at three predetermined heated positions marked with green crossing lines in Fig. 3b, were selected to be heated. Keeping the same heating time of 1 minute, the corresponding result was obtained. Visibly, the nanoparticles were sintered into three mounds around the three thermal points, and the corresponding size increased. As the left nanomound, mark in red rectangle, is mainly dependent on nanoparticles distribution and heat spot location. And comparing with previous morphology, the nanomound had greater height at the thermal spot of AFM probe tip, which indicates that the molten nanoparticles move toward the hot spot position. For further studying the flowability and surface tension effect of molten nanoparticles, with the same laser power of 64 mW and longer heating time of 3 minutes, the secondary operation was carried out at the center of elongated nanomound marked in red rectangle. As the nanospot welding result, the elongated nanomound formed a bigger circular mound, showing that the molten nanoparticles flow to the thermal spot position and keep the circular shape due to the surface tension effect. In addition, poor hydrophilicity, depended on the silicon material and its roughness, can also affect the shape of nanomound. Consequently, the experiments not only show that the nanospot welding process of silver nanoparticles can be achieved with the thermal AFM probe irradiated by optical fiber probe laser, but also provide the strong evidence for subsequent nanointerconnection experiments of CNTs. In addition, the broadening of silver particles, not selected for heating, appeared in the nano-welding process. It is attributed to that the optical fiber probe laser could also illuminate the surrounding silver nanoparticles when it irradiated the AFM probe tip. The surface plasmon appeared, the near-field enhancement effect caused the generation of broadening the under larger laser power, without the melting process of nanoparticles and merging together of the adjacent nanoparticles. So the laser power should be controlled during the nano-welding process of CNTs.

Before the nanospot welding process of CNTs, the CNTs sample also should be prepared. Adopting the similar treatment method to silver nanoparticles, the dispersion solution of CNTs with the outer diameter of approximate 7 nm and the purity of 95%, was diluted with ethanol absolute according to the volume ratio of 1 : 1000. For better dispersion effect, the mixed solution was treated with ultrasonic instrument about 2 hours, accompanying the heating operation at approximate 50 °C. And after 10 minutes' standing, supernatant liquid in the centrifuge tube was got as initial sample. In addition, the above dispersion solution of silver nanoparticles was diluted and dispersed with ethanol absolute according to the volume ratio of 1 : 5, and then the initial CNTs dispersion sample and silver nanoparticles

dispersion solution were mixed in a volume ratio of 1 : 1. After the dispersion treatment of the mixed solution about 1 hour and 10 minutes' standing, the supernatant liquid was also injected with discharge gun, coated on the Si surface with spin coater, and dried with the flow of N_2, obtaining the final dispersion sample shown in Fig. 4a. A silver nanoparticle was at the connection position between the two CNTs, and the other one, marked in red rectangle, was slightly deviated from the axial center position of the two carbon nanotubes. Based on laser power settings in the above nano-welding experiments of nanoparticles, considering the effect of flowability of molten nanoparticles under larger laser power, the heating spot of AFM probe tip was precisely located at the axial center position which was marked with green crossing lines in Fig. 4a. In addition, based on the researches about excellent electrical property of carbon nanotubes,[45–48] using the molecular dynamics simulation method, CNTs can be well connected with high heating temperature and long heating time, which was studied in our previous reports.[49–51] So, according to the above nanospot welding effect under different power and heating time, the laser power and irradiation time were set to 40 mW and 3 minutes respectively. And in the nanospot welding experiments, the CNTs were well wrapped by molten nanoparticles with cooling treatment, which is shown in Fig. 4b. In addition, from the perspective of quantification, the silver nanoparticle, nano-welding dot and carbon nanotubes were measured in experiments, and the height of nano-welding dot becomes smaller with corresponding larger lateral size in Fig. 4c. Due to size limitations of carbon nanotubes and the nano-welding dot, and large contact resistance problems of nanoprobe measurements, so far the electrical properties testing experiments are still unable to be solved in the order of 10 nm with existing advanced technology. In addition, the mechanical strength also plays an important role in nanospot welding effect of the metallic carbon nanotubes. If the contact strength is not enough for good connection and external disturbance, the electrical property may be affected by various factors. So the mechanical strength of nano-welding dot was studied through the following the nanomanipulation. Through the measurement of nanodot, marked with number '4' in Fig. 4a, this nanodot height was approximately equal to the sum of the outer diameter of CNT and the diameter of silver nanoparticle, which indicates that the silver nanoparticle approximately adhered to the top of carbon nanotube due to surface effect with high surface energy. After the nano-welding process of carbon nanotubes, the longer carbon nanotube was applied with moderate force, shown in Fig. 4a. With the effect and direction of the applied force, the carbon nanotube was manipulated to move slightly to the left part based on vector scanning mode of AFM system, which is shown in Fig. 4b. So, the top part of carbon nanotube was exposed after the nanomanipulation. Visibly, because the adhesion effect is very small for the silver nanoparticles being on the top of carbon nanotube, the nanoparticle moved and placed in the right side of carbon nanotube with inertia and other reason, which indicates that this nanoparticle, although near to the thermal spot, was not significantly affected or melted by nanospot welding process of CNTs. And as the connection of CNTs, if the CNTs were not connected, the position of CNTs at the connection point can be changed under the pushing force of AFM probe. But, the position of CNTs at the connection was not changed, and the interconnection of CNTs was not also affected by manipulation, showing that the CNTs were firmly fixed on the substrate by the molten Ag nanoparticles. Comparing the two nanoparticles at the heating point, marked with red rectangle in Fig. 4a and b, the two silver nanoparticles did not form an integral mound according to the above flowability research of molten nanoparticles under smaller laser power in Fig. 3.

In the above nanospot welding process, the two carbon nanotubes were connected by one Ag nanoparticle and nano-welding process would be influenced by oxidation of Ag nanoparticle on the AFM experimental platform in atmospheric environment. Considering the nanomanipulation of nano-objects and the controllable adjustment of the distance between the optical fiber probe and AFM probe, the nanomanipulation system based on nanorobot with AFM probe, with the similar software monitoring system, was developed without the function of scanning and imaging on scanning electron microscopy (SEM) platform. And the similar nanospot welding was performed in the vacuum environment with SEM. The same sample was selected in nano-welding process and the corresponding result was shown in Fig. 5. Before the

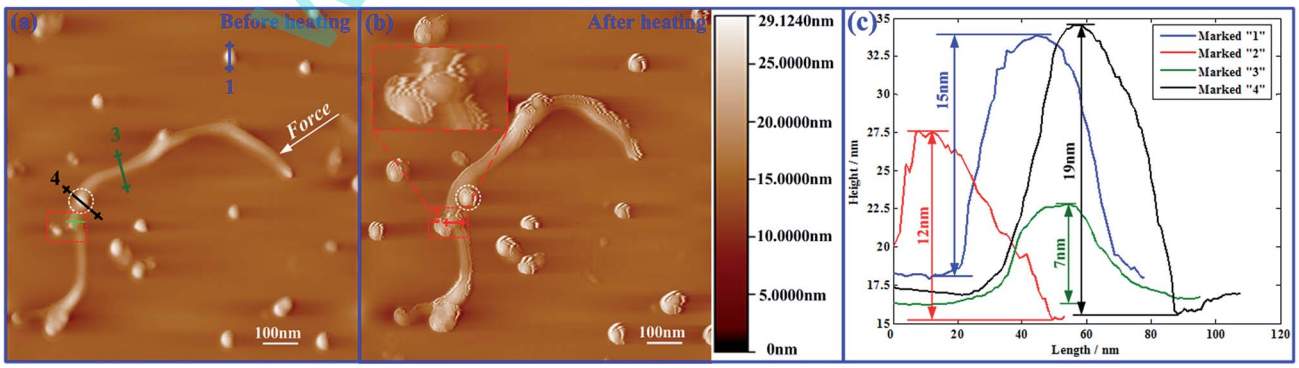

Fig. 4 Experimental interconnection of carbon nanotubes (a) before heating and (b) after heating treatment based on AFM probe tip illuminated by fiber probe laser (40 mW) with (c) the corresponding height sizes.

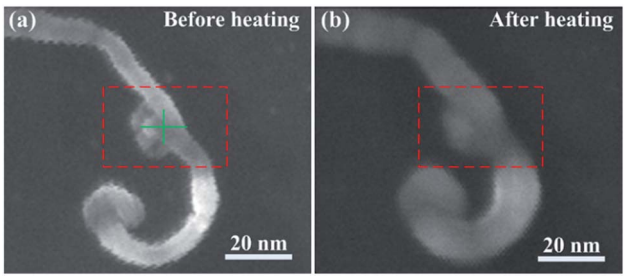

Fig. 5 SEM images of carbon nanotubes interconnection with the melting process of Ag nanoparticles (a) before heating and (b) after heating treatment based on AFM probe tip illuminated by fiber probe laser (laser power: 40 mW; irradiation time: 3 minutes).

heating operation, CNTs junction point with Ag nanoparticles was got, and its center position was selected as the heating point of the thermal AFM probe tip irradiated by optical fiber probe laser. With the same laser power of 40 mW and irradiation time of 3 minutes, the two carbon nanotube were well connected with good quality of nano-welding spot. At the connection position, the Ag nanoparticles melted and wrapped the CNTs connection point as a whole with smooth nanostructure. Maybe, due to the thermal effect of optical fiber probe laser, the CNTs curled with shorter axial size and larger radial size. The nanospot welding experiments fully not only show that the interconnection operation of CNTs can be effectively achieved by the thermal AFM probe tip irradiated by optical fiber probe laser, but also provide a promising technical approach for nanospot welding.

4. Conclusion

The new nanospot welding method, using AFM probe tip irradiated by optical fiber probe laser, was proposed based on the near-field enhancement effect. In theoretical simulations, the surface plasmon resonance and edge enhancement phenomenon affect the electric field distribution of the metallic AFM probe with the secondary enhancement phenomenon in the near-field region of optical fiber probe aperture, then to achieve the stable high temperature for the nanosoldering operations. In the nanospot welding experiments, setting up the system platform, the silver nanoparticles can be sintered into the larger mound at the thermal position of AFM probe irradiated by optical fiber probe laser. And the nanomounds can be easily formed with high laser power and long irradiation duration time, accompanying the obvious flowability. So, based on the new nanospot welding method, the carbon nanotubes were well wrapped by molten nanoparticles with cooling treatment without affecting the surrounding other nanoparticles through mechanical nanomanipulation treatment, not only proving that the interconnection operation of CNTs can be effectively achieved by the thermal AFM probe tip irradiated by optical fiber probe laser, but also providing a promising technical approach for nanospot welding.

Acknowledgements

This project was supported by the National Natural Science Foundation of China (51275122), China Postdoctoral Science Foundation (2014M562397), State Key Laboratory of Surface Physics and Department of Physics, Fudan University (KF2014_04), Fundamental Research Funds for the Central Universities (xjj2015009). All the authors gratefully acknowledge their support.

References

1 Semiconductor Industry Association, International Technology Roadmap for Semiconductors, 2012, Update, http://public.itrs.net/.
2 S. Iijima, *Nature*, 1991, **354**, 56–58.
3 M. S. Fuhrer, J. Nygård, L. Shih, M. Forero, Y. G. Yoon, M. S. C. Mazzoni, H. J. Choi, J. Ihm, S. G. Louie, A. Zettl and P. L. McEuen, *Science*, 2000, **288**, 494–497.
4 G. F. Close, S. Yasuda, B. Paul, S. Fujita and H. S. P. Wong, *Nano Lett.*, 2008, **8**, 706–709.
5 W. J. Park, K. J. Choi, M. H. Kim, B. H. Koo, J. L. Lee and J. M. Baik, *ACS Appl. Mater. Interfaces*, 2013, **5**, 6802–6807.
6 A. Malapanis, V. Perebeinos, D. P. Sinha, E. Comfort and J. U. Lee, *Nano Lett.*, 2013, **13**, 3531–3538.
7 A. D. Franklin, S. O. Koswatta, D. B. Farmer, J. T. Smith, L. Gignac, C. M. Breslin, S. J. Han, G. S. Tulevski, H. Miyazoe, W. Haensch and J. Tersoff, *Nano Lett.*, 2013, **13**, 2490–2495.
8 O. Cretu, A. R. Botello-Mendez, I. Janowska, C. Pham-Huu, J. C. Charlier and F. Banhart, *Nano Lett.*, 2013, **13**, 3487–3493.
9 H. Jiang, K. Moon and C. P. Wong, *Microelectron. Reliab.*, 2013, **53**, 1968–1978.
10 D. Eder, *Chem. Rev.*, 2010, **110**, 1348–1385.
11 A. A. Balandin, *Nat. Mater.*, 2011, **10**, 569–581.
12 A. D. Franklin, M. Luisier, S. J. Han, G. Tulevski, C. M. Breslin, L. Gignac, M. S. Lundstrom and W. Haensch, *Nano Lett.*, 2012, **12**, 758–762.
13 M. M. Shulaker, G. Hills, N. Patil, H. Wei, H. Y. Chen, H. S. P. Wong and S. Mitra, *Nature*, 2013, **501**, 526–530.
14 M. M. Shulaker, J. V. Rethy, T. F. Wu, L. S. Liyanage, H. Wei, Z. Li, E. Pop, G. Gielen, H. S. P. Wong and S. Mitra, *ACS Nano*, 2014, **8**, 3434–3443.
15 M. Terrones, F. Banhart, N. Grobert, J. C. Charlier, H. Terrones and P. M. Ajayan, *Phys. Rev. Lett.*, 2002, **89**, 075505.
16 I. Jang, S. B. Sinnott, D. Danailov and P. Keblinski, *Nano Lett.*, 2004, **4**, 109–114.
17 F. Banhart, *Nano Lett.*, 2001, **1**, 329–332.
18 A. V. Krasheninnikov, K. Nordlund, J. Keinonen and F. Banhart, *Phys. Rev. B: Condens. Matter Mater. Phys.*, 2002, **66**, 245403.
19 A. V. Krasheninnikov and K. Nordlund, *J. Appl. Phys.*, 2010, **107**, 071301.
20 R. D. Johnson, D. F. Bahr, C. D. Richards, R. F. Richards, D. McClain, J. Green and J. Jiao, *Nanotechnology*, 2009, **20**, 065703.

21 C. Chen, L. Yan, E. S. W. Kong and Y. Zhang, *Nanotechnology*, 2006, **17**, 2192.
22 G. Shen, Y. Lu, L. Shen, Y. Zhang and S. Guo, *ChemPhysChem*, 2009, **10**, 2226–2229.
23 C. P. Dockendorf, T. Y. Choi, D. Poulikakos and A. Stemmer, *Appl. Phys. Lett.*, 2006, **88**, 131903.
24 C. P. Dockendorf, M. Steinlin, D. Poulikakos and T. Y. Choi, *Appl. Phys. Lett.*, 2007, **90**, 193116.
25 W. Wu, A. Hu, X. Li, J. Q. Wei, Q. Shu, K. L. Wang, M. Yavuz and Y. N. Zhou, *Mater. Lett.*, 2008, **62**, 4486–4488.
26 Y. Peng, T. Cullis and B. Inkson, *Nano Lett.*, 2008, **9**, 91–96.
27 S. Guo, *Nanoscale*, 2010, **2**, 2521–2529.
28 Q. Cui, F. Gao, S. Mukherjee and Z. Gu, *Small*, 2009, **5**, 1246–1257.
29 C. T. Gibson, S. Carnally and C. J. Roberts, *Ultramicroscopy*, 2007, **107**, 1118–1122.
30 A. D. Slattery, A. J. Blanch, J. S. Quinton and C. T. Gibson, *Nanotechnology*, 2013, **24**, 235705.
31 J. Martinez, T. D. Yuzvinsky, A. M. Fennimore, A. Zettl, R. García and C. Bustamante, *Nanotechnology*, 2005, **16**, 2493.
32 S. M. Huang, M. H. Hong, Y. F. Lu, B. S. Lukỳanchuk, W. D. Song and T. C. Chong, *J. Appl. Phys.*, 2002, **91**, 3268–3274.
33 A. Chimmalgi, D. J. Hwang and C. P. Grigoropoulos, *Nano Lett.*, 2005, **5**, 1924–1930.
34 A. Chimmalgi, C. P. Grigoropoulos and K. Komvopoulos, *J. Appl. Phys.*, 2005, **97**, 104319.
35 C. Girard and A. Dereux, *Rep. Prog. Phys.*, 1996, **59**, 657.
36 S. Sangu, K. Kobayashi and M. Ohtsu, *J. Microsc.*, 2001, **202**, 279–285.
37 L. Novotny and S. J. Stranick, *Annu. Rev. Phys. Chem.*, 2006, **57**, 303–331.
38 L. Novotny and N. van Hulst, *Nat. Photonics*, 2011, **5**, 83–90.
39 J. Cui, L. Yang and Y. Wang, *Laser Phys.*, 2013, **23**, 076003.
40 E. D. Palik, *Handbook of optical constants of solids*, Academic press, 1998.
41 F. Demming, J. Jersch, K. Dickmann and P. I. Geshev, *Appl. Phys. B: Lasers Opt.*, 1998, **66**, 593–598.
42 P. I. Geshev, F. Demming, J. Jersch and K. Dickmann, *Appl. Phys. B*, 2000, **70**, 91–97.
43 P. I. Geshev, F. Demming, J. Jersch and K. Dickmann, *Thin Solid Films*, 2000, **368**, 157–163.
44 J. Cui, L. Yang and Y. Wang, *Rare Met. Mater. Eng.*, 2014, **43**, 369–374.
45 L. Forro and C. Schoenenberger, *Physical properties of multi-wall nanotubes*, Springer, Berlin, Heidelberg, 2001.
46 C. H. Kiang, J. S. Choi, T. T. Tran and A. D. Bacher, *J. Phys. Chem. B*, 1999, **103**, 7449–7451.
47 M. Ferrier, A. Kasumov, R. Deblock, S. Guéron and H. Bouchiat, *C. R. Phys.*, 2009, **10**, 252–267.
48 E. Borowiak-Palen, M. H. Ruemmeli, T. Gemming, T. Pichler, R. J. Kalenczuk and S. R. P. Silva, *Nanotechnology*, 2006, **17**, 2415.
49 J. Cui, L. Yang and Y. Wang, *Appl. Surf. Sci.*, 2013, **264**, 713–717.
50 J. Cui, L. Yang, L. Zhou and Y. Wang, *ACS Appl. Mater. Interfaces*, 2014, **6**, 2044–2050.
51 J. Cui, L. Yang, Y. Wang, X. Mei, W. Wang and C. Hou, *ACS Appl. Mater. Interfaces*, 2015, **7**, 2294–2300.